Comparative study of the uncertainty of stereoscopic micro-PIV, wavefront-deformation micro-PTV, and standard micro-PIV

Christian Cierpka[1], Massimiliano Rossi[1], Rodrigo Segura[1], Francesco Mastrangelo[2], Christian. J. Kähler[1]

1: Institute of Fluid Dynamics and Aerodynamics, Universität der Bundeswehr München, Neubiberg, Germany, [Christian.Cierpka, Massimiliano.Rossi, Rodrigo.Segura, Christian.Kaehler]@unibw.de
2: Department of Mechanics, Politecnico di Torino, Torino, Italia, Francesco.Mastrangelo@polito.it

Abstract In this paper a comparative study is presented to assess the uncertainty of two methods for 3C3D velocimetry in microscopic flows: stereoscopic micro-particle image velocimetry (S-μPIV) and wavefront-deformation, or astigmatism, micro-particle tracking velocimetry (WD-μPTV). First, the main parameters affecting both methods' measurement uncertainty are identified, described and quantified. Second, the test case of flow over a backward-facing step is analyzed using both methods. For comparison standard 2D-2C μPIV measurements and numerical flow simulations are shown as well. Advantages and disadvantages of both methods are discussed.

1. Introduction

With the increasing complexity of microfluidic devices such as micro-mixers, micro-bioreactors and micro-heat exchangers, among others, three-dimensional flows become an important challenge. Ever since the μPIV (Particle Image Velocimetry) method was introduced by Santiago et al. (1998) as an experimental tool for the measurement of 2D-2C (two-dimensional, two components) velocity fields in microfluidic devices, it has become one of the most wide-spread techniques in microfluidics. However, there are some inherent limitations:

1. Due to the volume illumination, the minimal thickness of the measurement plane is determined by the imaging optics' depth of focus and thus limited to several μm.
2. Since the whole volume is illuminated, out of focus particles contribute also to the cross correlation (depth of correlation) and hence, bias the measurement (Rossi et al. 2010).
3. Only 2C-2D velocity fields can be measured.

The improvement and adaptation of the μPIV technique is still an ongoing process. A recent review of the state of the art of μPIV and of relevant applications was published by Lindken et al. (2009). The authors also discuss guidelines for the implementation of the technique in a broad field of different areas of research. Several methods have been proposed to extend the velocity reconstruction to the third component. Reviews about advanced 3D methods can be found by Lee and Kim (2009) and Cierpka et al. (2010).

One method consists of using different viewing perspectives. Stereoscopic μPIV (S-μPIV), derived from μPIV, is one of these methods and makes use of a stereoscopic microscope to observe the flow field in the measurement region from two slightly different viewing angles. The in-plane particle image displacement seen by two cameras under different angles within Δt can be used to estimate the in-plane velocity by 2D cross-correlation. The third component is then reconstructed by the in-plane velocities as will be explained in detail in section 2. Another approach is the tomographic reconstruction of the particle distribution in the volume, after which 3D cross-correlation is applied to obtain the 3D velocity field. Both methods need a very precise calibration and suffer from the small viewing angles applied (Lindken et al. 2006). Thus, especially the applicability of tomographic methods to microfluidic devices seems to be quite limited.

Recently, in-line holography (Kim and Lee 2009; Ooms et al. 2009) was applied to 3D velocity field measurements in microscopic channels. However, the reconstruction process is rather time

consuming and the optical setup has to be built with great care to have an acceptable accuracy of the out-of-plane velocity. To overcome the difficulties of the complex calibration procedure in holography and multi-camera techniques, a method using just one camera is favorable.
The depth coding via three pinholes is such a technique, estimating the particle's depth position via two dimensional images (Pereira et al. 2000; Willert and Gharib 1992). With the three pinholes, a particle is imaged as a triplet. The distance between the edges of the triplet is related to the depth position. This concept is more robust than holography and was successfully applied to micro fluidics by Yoon and Kim (2006). Aside from masking the optics, there are other methods to break the axis symmetry of an optical system. This allows for the coding of the depth position of particles in a 2D image. By later reconstruction of the particles' position in real space, the velocity field can be evaluated by correlation algorithms or tracking methods. So far, diffraction gratings for multi-planar imaging (Angarita-Jaimes et al. 2006), a bended dichroic mirror (Ragan et al. 2006), an optical filter plate at an angle (van Hinsberg et al. 2008), and cylindrical lenses (Hain et al. 2009; Chen et al. 2009) were successfully used for this purpose in microscopic flows. The approach based on cylindrical lenses, especially, is a very powerful and simple method, which allows for the extension of existing 2D measurement systems to fully 3D measurements. A big advantage of this approach is the possibility to adjust the measurement depth and resolution by changing the focal length of the cylindrical lens.
Therefore, the S-μPIV approach and the astigmatism or wavefront-deformation PTV will be studied and discussed in the following. In order to determine the accuracy and uncertainty of both techniques, measurements of the flow over a backward facing step will be compared with standard μPIV as well as numerical simulations.
The backward facing step flow was chosen, since it offers a velocity field that is well known and mainly one directional prior to the step and has a very pronounced out-of-plane component shortly beyond the step. Other groups have also verified their 3D measurement methods with backward facing step flows (Chen et al. 2009; Yoon and Kim 2006; Bown et al. 2006). A combined stereo PIV/PTV approach was used by Bown et al. (2006). They measured the flow over a 232μm step in a channel 466μm high channel. Glycerol was used as working fluid, resulting in $Re_h \approx 0.004$. The flow was investigated with stereoscopic μPIV at 23 different planes in the *z*-direction. The accuracy of the correlation based results was found to be limited by the misalignment or non-overlapping of the two focal planes of the stereo microscope. To improve the accuracy, a super resolution PTV approach was applied. Using a PTV algorithm allows to restrict valid measurements only to strongly focused particles which decreases the effect of the depth of correlation. The authors reported uncertainties for the averaged vector map in the order of 0.35μm/s (3% of the mean velocity), for the in-plane components, and 0.82μm/s (7% of the mean velocity) for the out of plane component of the correlation based velocity estimation. The uncertainty was decreased to 2% and 3% for the in-plane and out-of-plane velocity, respectively, with the PTV algorithm. Unfortunately, the way the uncertainties were determined was not reported and a comparison is therefore difficult.
Chen et al. (2009) used a cylindrical lens with f_c = 500mm to measure a 600μm range in a 170μm backward facing step, inside a 500μm high channel. The uncertainty for the depth position was reported to be 2.8μm for the calibration images. Unfortunately no uncertainty of the single measurements was given. The measured RMS value of the velocity was 3.3μm/s, even though 2.8μm/s was expected from the measurement uncertainty. This is above one third of u_∞. The investigated Reynolds number was $Re_h \approx 0.0015$. The images were therefore taken in single frame mode, probably with continuous laser light illumination, and are of higher quality than double frame images with very short laser light pulses. The separation time between successive images in the study was Δt = 2s. The authors stated that 3,000 images were acquired, which takes 100 minutes. This and the very low Reynolds number is far beyond realistic 'Lab-on-a-chip' applications which range in the order of Re_h = 1…100 and require double frame images, which suffer from large noise levels.

2. Experimental setup

2.1 Backward Facing step and conventional µPIV

All experiments were performed in the same microchannel to avoid variations in the boundary conditions. The microchannels are fabricated out of elastomeric polydimethylsiloxane (PDMS) on a 0.6mm thick glass plate by the Institute for Microtechnology of the Technical University Braunschweig. They possess inlet and outlet cross-sectional areas of $500\times150\mu m^2$ and $500\times200\mu m^2$ respectively. The channel was approximately 30mm in length, with the backward-facing step at about 15mm from the inlet to assure fully developed flow conditions. The flow in the channel was seeded with polystyrene latex particles, fabricated by Microparticles GmbH. The particle material was pre-mixed with a fluorescent dye, and the surface of the latex micro-spheres was later PEG modified to make them hydrophilic. Agglomeration of particles at the channel walls can be avoided by this procedure, allowing for long duration measurements without cleaning the channels or even clogging. The diameter of the particles was narrowly distributed with a mean diameter of d_P = 2µm for the WD-µPTV measurements and d_P = 1µm for all PIV measurements. The fluid was distilled water, which was pushed by a precision Nexus 3000 syringe pump (manufactured by Chemix) with constant flow rate through the channel. The Reynolds number based on the step height was Re_h = 3.75 and based on the hydraulic diameter of the inlet Re_{HD} = 17.3.
For the illumination of the particles, a two cavity frequency doubled Litron Nano S Nd:YAG laser system was used. The image recording was done using the DaVis 7.4 software package from LaVision. The images were acquired in double exposure mode, where the camera shutter is activated two times. The time delay between the two successive frames was set to Δt = 200µs. 1000 images were recorded at each *z*-position for all three techniques.
The WD-µPIV measurements, as well as the 2D-2C conventional µPIV measurements, were performed using an Axio Observer Z.1 inverted microscope by Carl Zeiss AG with a LD-Plan Neofluar objective with numerical aperture of NA=0.4 and a magnification of M=20x.
To reconstruct the velocity field in the volume from conventional PIV, the raw image pairs were preprocessed and cross correlated. Preprocessing consisted of subtracting the sliding minimum over time, and then in space to decrease non-uniformities and back-reflections. These steps are followed by a bandwidth filter and constant background subtraction, used to sort out particle agglomerations and eliminate the remaining background noise. 2D velocity fields were measured for seven planes inside the channel. The image pairs were cross-correlated with the DaVis 7.4 software package from LaVision. A normalized multi-pass algorithm with interrogation window sizes of 32 × 32 pixels was used with 50% overlapping of the interrogation windows with an average of 3-5 particle images per window. Since the flow was laminar and stationary, the vector fields from each plane were averaged. For the numerical flow simulation the microchannel was modelled with a solid modeller to extract the microchannel boundaries: the boundaries were meshed in CD-adapco STAR-CCM+ 4 and a finite volume model was set for a laminar and viscid fluid with a constant density (water). The computational domain exceeds 600,000 hexahedral cells. In the step region, four times the channel width, the mesh size was equal to 6.25µm (1/80 of step width) to ensure an optimal velocity resolution. The no-slip condition was set at the boundaries of the computational domain. At the inlet the velocity was set matching Re_h number of the experiment. At the outlet the pressure was set to a reference value. To avoid entrance effects, two flow extensions were located at the inlet and the outlet: uniform boundary conditions are set at a distance of twenty times the channel width. The steady solution converged using the implicit solver in 500 steps: the relative errors of residuals of continuity and momentum were less than 10^{-6}.

2.1 Stereoscopic PIV

For the S-μPIV measurements, an upright stereoscopic microscope, with a common main objective (CMO) lens configuration (Leica M165 FC) was used. The CMO design uses a large diameter objective lens, through which both the left and right channels view the object. The optical axis of the objective is normal to the object plane, therefore there is no inherent tilt of the image at the CCD focal plane, and the left and right images are viewed by the CCD cameras, theoretically, with no convergence (Fig. 1).
The corresponding direct linear transform for the conversion between the image and object spaces can be derived using geometric optics:

$$\begin{aligned}
\Delta X_1' &= M(\Delta x + \tan\theta_1 \cos\alpha_1 \cdot \Delta z) \\
\Delta Y_1' &= M(\Delta y + \tan\theta_1 \sin\alpha_1 \cdot \Delta z) \\
\Delta X_2' &= M(\Delta x + \tan\theta_2 \cos\alpha_2 \cdot \Delta z) \\
\Delta Y_2' &= M(\Delta y + \tan\theta_2 \cos\alpha_2 \cdot \Delta z)
\end{aligned} \tag{1}$$

where (ΔX_1', ΔY_1') and (ΔX_2', ΔY_2') are the projection of a displacement vector (Δx, Δy, Δz) in the image space of camera 1 and camera 2 respectively, and θ_1, θ_2, α_1 and α_2 are angles as defined in Fig. 1. Equation (1) is derived under the assumption that the working distance of the lens is much larger than the displacement in the axial direction.
In a real system, the transform is typically more complex than the one in equation (**1**) due to distortions and aberrations induced by imperfections of the lens or by refraction between different media (e.g., glass and water of the microchannel). Therefore, an empirical calibration is required. For the presented measurements, a stereo-lens Planapo 2x, with NA=0.282 was used, in combination with the internal zoom lens system of the microscope, which was set to achieve a total magnification of 20x, at the CCD of the cameras. Images were taken with two double-frame cameras with 4k × 2.6k pixels CCD sensors (PCO 4000).
The calibration was performed using a calibration plate with a grid reticule where the lines were 50μm apart from each other. The grid was displaced along the axial direction, with steps of 2μm, using a piezoelectric stage (PZ 400 SG, Piezosystem Jena GmbH) with a resolution of 7.5 nm. A multi-plane polynomial function of third order was used to fit the calibration curves (displacement of the grid crosses in the image space of cameras 1 and 2 as a function of the axial position of the grid). A self-calibration procedure (Kähler et al. 1998) was subsequently used to account for further distortions introduced by the geometry of the step channel.

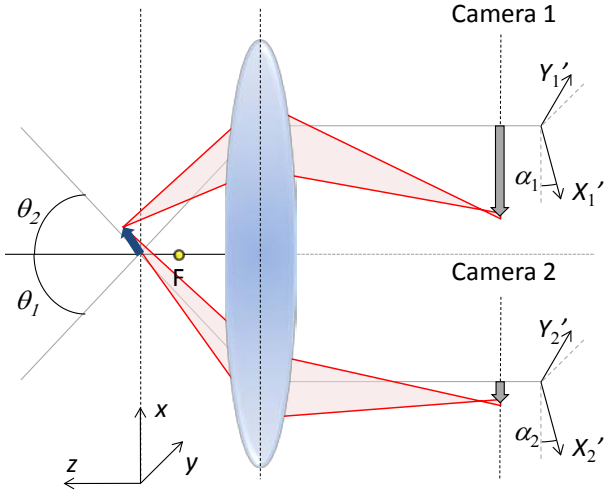

Fig. 1 Schematic of geometric optics for a stereoscopic microscope with a CMO design

A major problem in S-μPIV measurements is given by the possible misalignment of the measurement volumes of the two cameras caused by optical aberrations and imperfections in the construction of the microscope. In S-μPIV, as well as in μPIV, volume illumination is used and the measurement volume observed by one camera corresponds to the respective focal plane. The thickness of the measurement volume can be estimated using the depth of correlation (Olsen and Adrian 2000). As a consequence of the misalignment, a bias error occurs, especially when velocity gradients are present, since the evaluated 3D velocity vectors result from the recombination of the 2D velocity fields observed by cameras 1 and 2, under the assumption that they are taken in the same measurement volume. This error cannot be corrected since it inherently depends on the design and construction of the microscope.

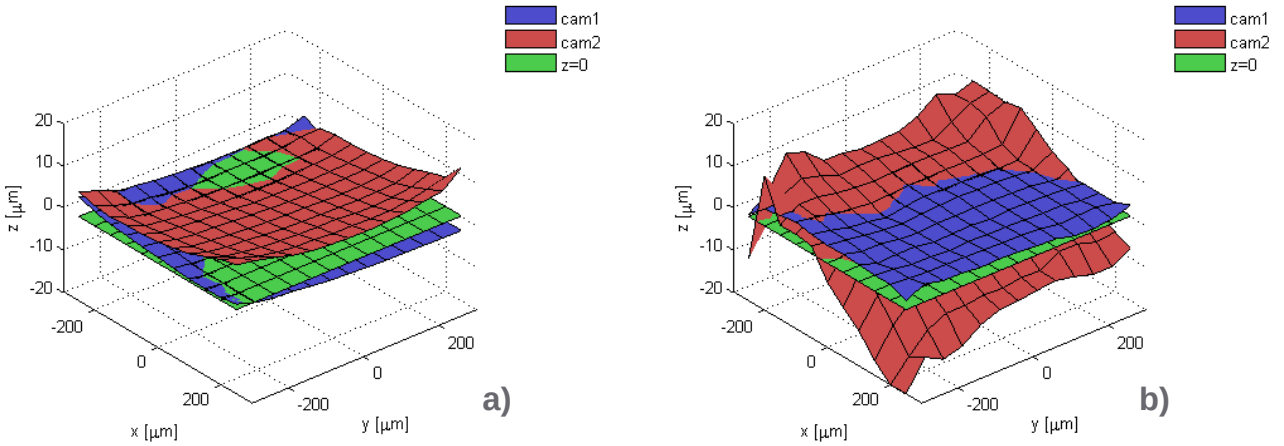

Fig. 2 Reconstruction of the focal planes for camera1 and 2 in air (a) and water (b)

In order to quantify the misalignment, the focal planes of cameras 1 and 2 were reconstructed taking images of the calibration plate at different heights and using a local focus function based on the variance of image intensity (Sun et al. 2004). The procedure was repeated with the calibration plate in air and immersed in a microchannel, analogous to the one used for the backward-facing step measurements, filled with water. The reconstructed focal planes for cameras 1 and 2 in air and water are reported in Fig. 2.

It can be observed that the centers of the focal planes are curved and overlap only partially, even when the finite thickness of the measurement volume is considered. Particularly for the case in water, in the region where the velocity measurements on the backward-facing step were taken, a mean difference of 4.1μm was estimated between the two focal planes, with a maximum of 11.2μm. This error is only negligible when the depth of the measurement volume is large compared to the misalignment. However, an additional error is introduced by averaging the velocity measurement through the depth of correlation in this case. For this set-up, using 1μm diameter particles, the depth of correlation was estimated to be equal to 36μm, which means that in the worse case one-third of the measurement thickness was not correlated. This can already lead to substantial errors (Kähler 2004).

With regards to the PIV analysis, the images were first pre-processed using a background sliding minimum filter for background removal and a smoothing median filter for image random noise reduction. Subsequently, a correlation averaging was run over 1000 images per plane, using a multipass algorithm with final interrogation window of 64×64 pixels and a 50% overlap. The vector fields were recombined using the empirical calibration to reconstruct the 3rd velocity component. The results were later organized on a Cartesian grid with the same grid size as the results of the conventional μPIV, with $\Delta x = \Delta y = 15\mu m$ and $\Delta z = 29\mu m$.

2.2. Astigmatism PTV

The depth coding of the particle position on the images is achieved by a cylindrical lens with a focal length of f_c = 100 mm. The same setup was used by Cierpka et al. (2010). This cylindrical lens was directly placed in front of the CCD chip. The curvature of the cylindrical lens only acts in one direction and causes two focal planes in the *x*- and *y*-axis to be formed. For the setup used here, these planes are separated by Δz = 45.2µm in the measurement volume. Particles that are close to one focal plane, e.g. the *x*-axis focal plane, will give a small and sharp image in that axis. They are now far from the in-focus plane in *y*-direction and result in defocused, larger images in the *y*-axis. Thus, an elliptical image is formed on the CCD chip, with a small horizontal axis, denoted as a_x, and a large vertical axis, denoted as a_y. If a particle is closer to the other focal plane, a_y becomes smaller than a_x. By a calibration procedure a_x and a_y can now be related to the actual *z*-position in the measurement volume. The axis a_x and a_y are determined by using an autocorrelation based algorithm with subpixel accuracy, which gives reliable results for particle images with a_x, $a_y > 3$ pixel. The error made by the algorithm was evaluated based on synthetic images to be less than 0.01 pixels for a_x and a_y. The resulting error from the algorithm is, in that case, less than 0.002µm in *z*-direction and can be neglected.

The position in the *xy*-plane is determined by a wavelet based procedure (Cierpka et al. 2008), which gives reliable results with subpixel accuracy up to high background noise levels. The ratio between background and signal intensity was below 0.1 for the measurements presented, which gives an error of 0.05 pixels for the position. This relates to an absolute error of 0.031µm in the *x*-direction and 0.038µm in the *y*-direction. For the final procedure, image preprocessing is applied to the images. First, a sliding minimum over time is subtracted to remove background noise. Smoothing and segmentation filters are then used to highlight regions of possible particle candidates. Based on this initial guess for particle positions, the algorithm determines a_x, a_y, *x* and *y* in the originally background-subtracted images. For more information on the algorithm, the interested reader is referred to Cierpka et al. (2010).

As for the stereoscopic PIV, the uncertainty of the following results is strongly affected by the accuracy of the calibration. In previous studies, the calibration of the depth position was built on the differences of the axis a_x-a_y (Chen et al. 2009) or on the ratio a_x/a_y (Cierpka et al. 2010). Both methods showed good results in the region between the two in-focus planes but are ambiguous beyond this region. The measurement depth would therefore be limited to the region between the two in-focus planes. Since the particles are rather narrowly distributed in size and the quality of the fluorescent dye allows detecting strongly defocused particles, it was possible to extend the measurement depth using the values for the axis a_x and a_y directly. Using Gaussian approximation of the intensity distribution of the particle images, the image diameter d_I can be estimated according to Olsen and Adrian (2000).

$$d_I = \sqrt{M^2 {d_P}^2 + 5.95(M+1)^2 \lambda^2 {f^{\#}}^2 + \frac{M^2 z^2 D^2}{(s_0 + z)^2}} \tag{2}$$

where M denotes the optical magnification, λ the wavelength, $f^{\#}$ the focal number of the lens and D the lens aperture. Equation (2) can be simplified and used to describe the particle images' width a_x and height a_y as

$$a_x = \sqrt{{a_{\min x}}^2 + C_x (z - z_{ax\min})^2} \qquad a_y = \sqrt{{a_{\min y}}^2 + C_y (z - z_{ay\min})^2}. \tag{3}$$

From scanning a particle sample in the *z*-direction, it turns out that the minimum axis width and height are equal, $a_{\min x} = a_{\min y} = a_{\min}$ to an acceptable extent. Also, the constant $C_x = C_y = C$ for a sample of narrow distribution of particle diameters (Cierpka et al. under review). The distance

between the two focal planes is determined to be $\Delta z = |z_{ax\,\min} - z_{ay\,\min}| = 45.2\mu m$. Since between the two focal planes at ($z_{ax\,\min}$+ 0.5 Δz), the width and height are equal ($a_x = a_y$), equation (2) is left with only one unknown value, *C*, which can be evaluated. The particle's position can now be calculated according to

$$z(a_x) = \pm\sqrt{\frac{a_x - a_{\min}}{C}} + z_{ax\,\min} \qquad z(a_y) = \pm\sqrt{\frac{a_y - a_{\min}}{C}} + z_{ay\,\min}. \tag{4}$$

For ideal conditions, two of the four values are equal and give the depth position of the particles. However, due to higher order image aberrations, uncertainties in the particle size distribution, and the determination of their width and height, the data points scatter around the ideal solution. To preserve ambiguity, the average value of $z(a_x)$ and $z(a_y)$ for the two closest positions is estimated as the *z*-position of the particle. The standard deviation between the estimated particle position z_{est} and the position according to equation (4) gives an impression about the uncertainty of a single measurement and was calculated to be $\sigma_{(z\text{-}zest)} = 3.02\mu m$. Using this calibration, the maximum measurement depth was 112µm. Therefore, the position uncertainty in the depth direction of a single measurement, without traversing, is 5.3%. However, for a single measurement this would result in an uncertainty of about 15mm/s. To compare the results one has to consider, that for the cross correlation about, 6 to 10 particle images should be present in an interrogation area. The data was later interpolated of a Cartesian gird and showed a good convergence of the mean value in a volume element. The difference between the mean value, taking a certain number $i=I$ of data points as well as all data points $i=N$ that belong to one grid volume into account $\varepsilon_w = |\Sigma w_{i=I}/I - \Sigma w_{i=N}/N|$, is a measure of convergence. Taking 6 particle images the difference is just ε_w = 1.2mm/s. The average number of data points that contribute to a grid volume element was 40, which gives a difference ε_w = 0.24mm/s.

Knowing the particle position in the volume at two different time instants *t* and $t + \Delta t$ allows for an estimation of the first order approximation of the particles' velocity. A simple nearest neighbor PTV algorithm was applied. To make this algorithm work robustly, the particle's displacement should be smaller than the average distance between particle images (Maas et al. 1993). The measurement volume depth depends on the microscope magnification and focal length of the cylindrical lens, as well as on the detection level of the camera, the power of the laser, and the quality of the fluorescent dye. For the study presented here, approximately 50% of the data points are within a span of 33.7 µm, centered at the mid-point between the two focal planes and 90% fall between a span of 64.2 µm. To cover the whole channel, overlapping data was acquired at seven different *z*-positions. For each *z*-level, around 50,000 good particle pairs were identified and the average number of particle images per frame was 50. Less particle images per frame occur for the measurements closer to the wall, since a part of the measurement volume was already outside of the channel.

The data of all individual particles was filtered by a global histogram filter in order to remove strong outliers. A local universal outlier detection algorithm (Westerweel and Scarano 2005) was lately adapted to PTV data by Duncan et al. (2010). The authors proposed a weighting of the neighboring values by their distances. The normalized residuum or fluctuation at the position, r_0*, is given by equation (5), where *med*(.) is the median value of a quantity, d_i denotes the distance to the neighboring point and *u* the velocity.

$$r_0^* = \frac{\left| \frac{u_0}{med(d_i) + \varepsilon_a} - med\left(\frac{u_i}{d_i + \varepsilon_a} \right) \right|}{med\left| \frac{u_i}{d_i + \varepsilon_a} - med\left(\frac{u_i}{d_i + \varepsilon_a} \right) \right| + \varepsilon_a} \tag{5}$$

The adaptive tolerance ε_a is given by equation (6), using an absolute tolerance of ε of 0.5µm.

$$\varepsilon = \varepsilon_a \left(med\ \left(d_i \right) + \varepsilon_a \right) \tag{6}$$

Taking the closest 10 neighboring data points into account, only vectors with a normalized residuum of $r_0^* > 2$ for all coordinates are considered to be valid. By this procedure, 13% of outliers, at the most, were removed from a dataset. For better comparison with the other techniques, the data was then interpolated on a Cartesian grid with grid size $\Delta x = \Delta y = 20$µm and $\Delta z = 12.5$µm and 15% overlap, covering the whole channel close to the step.
Using this interpolation about 40 single PTV measurements contribute to the mean at a grid point. As a measure for the uncertainty of the measurements the standard deviation of the single measurements std(u_i-u_{mean}) can be taken. However, this quantity is strongly affected by the grid size in regions of high gradients. Therefore it was evaluated upstream of the step (x < -50µm), where a laminar channel flow profile is present, and v and w have a zero mean and the scatter of the single PTV data points is purely by the measurement technique. The mean standard deviation for in that region was 0.7mm/s for v and 2.8mm/s for w. The uncertainty for the out-of-plane component is with 3.7% of u_∞ four times higher than for the in-plane component 0.9% of u_∞.

3. Results

In Fig. 3, slices of the streamwise velocity are shown for the simulation (right), the S-µPIV (middle) and the WD-µPTV (left). The flow direction is from left to right. Both 3D measurement techniques show the expected velocity profiles for Poiseuille flow. The velocity is higher upstream of the step and then decreases because of the expansion of the channel. Within the u-component, the influence of the step is not very pronounced.

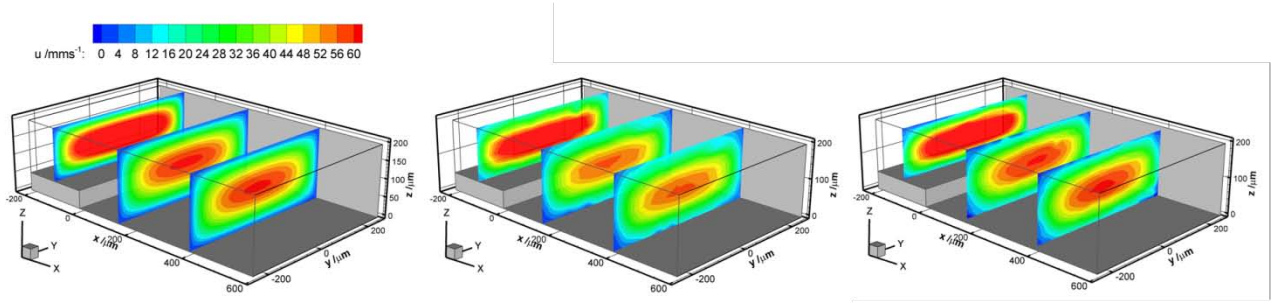

Fig. 3 Slices of the streamwise velocity for the simulation (right) the stereoscopic PIV (middle) and the astigmatism PTV (left).

In Fig. 4, the out of plane component is shown. Immediately after the step, the flow goes downward and follows the contour of the step. To quantify the overall agreement the velocity of the flow simulation was interpolated at the grid points of the experimental results. Based on this, the standard deviation of $|u_{exp}-u_{sim}|$ is given in the following table. For the in plane components the differences between simulation and results from S-µPIV and WD-µPTV are in the same order, but lower than for standard µPIV. For the out-of-plane component the best agreement can be achieved with the WD-µPTV technique.

	conventional PIV	stereoscopic PIV	WD-PTV
σ of $\lvert u_{exp}-u_{sim}\rvert$ /mms^{-1}	7.8	3.6	3.9
σ of $\lvert v_{exp}-v_{sim}\rvert$ /mms^{-1}	2.5	0.6	0.3
σ of $\lvert w_{exp}-w_{sim}\rvert$ /mms^{-1}	-	2.8	1.1

A pronounced recirculation was not seen either in the simulation, or in the measurements. Again, experimental results for both techniques show good qualitative agreement with the simulations.

Upward flow, further downstream from the step was estimated by the simulation to be at a maximum with w = 0.2 mm/s and could not be experimentally resolved. For the measurements with the stereo microscope, a region of downward flow is also found at x = 600µm, which is caused by the fact that the two focal planes do not overlap and therefore artificial out-of-plane motion is detected by the reconstruction. Nevertheless, the size of the downward flow region is well captured, whereas it is slightly underestimated with the WD-PTV technique.

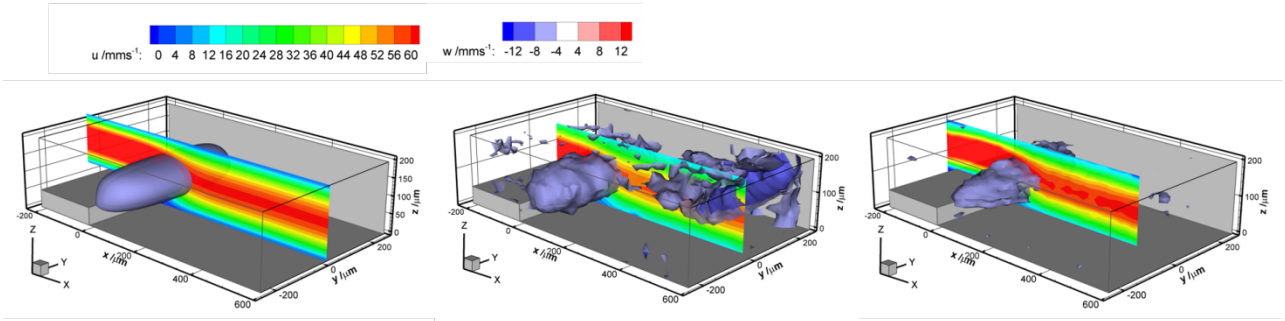

Fig. 4 Isosurfaces of the w-component of the velocity and a slice in the middle of the channel for the simulation (right) the stereoscopic PIV (middle) and the astigmatism PTV (left). The downward flow is evident for both measurements techniques.

A more detailed comparison is possible by using actual velocity profiles. Since the data is sampled on Cartesian grids, where the nodes do not overlap exactly, velocity values for certain coordinate ranges are presented. In Fig. 5 profiles for the streamwise velocity are shown for the center plane of the channel: immediately downstream of the step (right) and approximately 2 step heights downstream of the step (left).

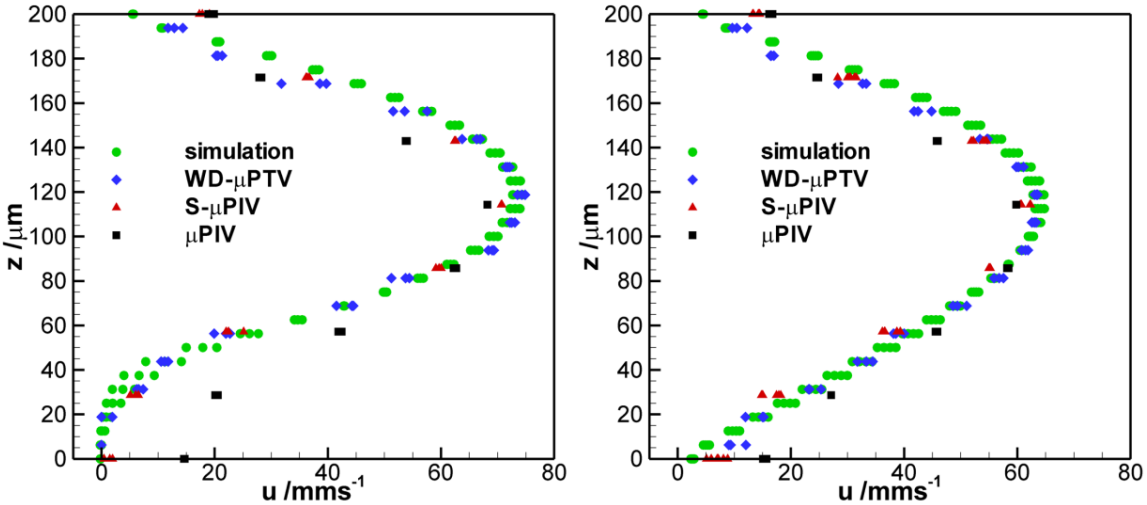

Fig. 5 Profiles of the u-component vs. z at 10<x<60µm; -21< y<21µm (right) and at 80<x<95µm; -21<y<21µm (left).

The lower velocity profile close to the step can be seen in all measurements. However, since no special care for the preprocessing of the images close to the step was taken, the velocity is overpredicted by conventional µPIV at the bottom of the channel. Since conventional and stereo µPIV is highly affected by the depth of correlation, if no special care is taken (Rossi et al. 2010), the velocities are averaged over a larger depth range and therefore underestimated in the middle of the channel, which can be clearly seen in the profiles. For the S-µPIV measurements, special care was given to image preprocessing, which decreases this effect and the profiles match the simulation considerably better in the middle of the channel. Nevertheless, close to the walls, the velocity is overestimated. For the conventional PIV a lot of the particle images of the low speed particles close to the step are taken out by the preprocessing. Therefore, the particles with higher velocity contribute much more to the correlation and the velocity is overpredicted. The PTV approach is not

affected by the bias due to depth of correlation and shows better results, especially in the regions of high gradients the results are closer to the numerical simulation compared to the correlation based methods.

The most challenging task lies in the measurement of the out-of-plane component and the in-plane component in regions with strong out-of-plane velocity. In Fig. 6, velocity profiles for u and w are shown for a region in the center of the channel, immediately above the step. The downward flow is clearly indicated by both 3D techniques. S-μPIV gives results very close to the simulation, whereas the maximum velocity compared to the simulation is underestimeted by 10% for WD-μPTV. This effect can be caused by the high gradients in that region. Using smaller tracer particles for the PIV measurements might produce better results. For the S-μPIV, a region of upward flow is detected for $x > 150$μm. This effect is not physical and is caused by non overlapping focal planes. The results for the WD-μPTV scatter much more, and show values smaller than $w = 0$. Nevertheless, these measurements are closer to the results of the simulation. On the right hand side of the same figure the streamwise velocity is presented. Conventional μPIV is included as well but shows poor performance in the region above the step. The boundary layer of the bottom wall, prior to the step, cannot be well resolved and the velocity measured is much too high, due to the depth of correlation. S-μPIV performs slightly better, but over predicts the velocity as well. The best match between experiments and simulation is achieved by the WD-μPTV although the velocity, $u \approx 17$mm/s, is higher than the one predicted by the simulation of $u \approx 13$mm/s.

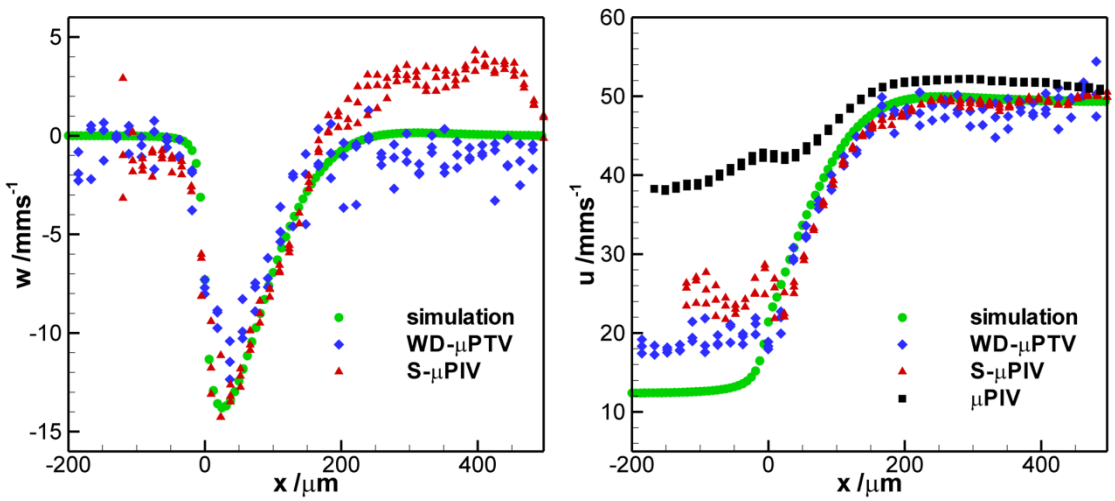

Fig. 6 Profiles of the u-component vs. x at 50<z<60μm; -21<y<21μm (right) and of the w-component at 50<z<60μm; -21<y<21μm (left).

4. Conclusion & Outlook

Standard μPIV becomes inaccurate in the analysis of 3D flow fields. In regions of high gradients and larger portions of out of plane flow the technique fails at providing reliable results. Both μPIV extensions, S-μPIV and WD-μPTV are capable of measuring the 3C velocity field. Whereas for S-μPIV the resolution in depth is given by the successive measurement planes, WD-μPTV provides information in the whole volume. Nevertheless, a larger uncertainty is related to the single PTV measurement. For mean values, the uncertainty decreases significantly. An advantage of the WD-μPTV technique, compared to the correlation based methods, is that the results do not suffer from the influence of the depth of correlation and a higher resolution in depth position can be achieved. The results of the WD-μPTV technique can be improved using a more sophisticated calibration, and by taking into account deviations in the image plane $z = f(a_x, a_y, x, y)$. For S-μPIV measurements, special care must be taken with the cameras' setup. The focus function has to be evaluated for both cameras in order to adjust them accordingly and minimize the error, or at least to know to what

extent the results will be biased. An automatic calibration procedure will be developed for the system presented here.

5. Acknowledgements

Financial support from Deutsche Forschungsgemeinschaft (DFG) in frame of the priority program SPP 1147 and the research group 856 is gratefully acknowledged. The authors would also like to thank Stefanie Demming at the Institute for Microtechnology at the Technical University of Braunschweig for their kind support in fabricating the micro channels.

6. References

Angarita-Jaimes, N., E. McGhee, M. Chennaoui, H. I. Campbell, S. Zhang, C. E. Towers, A. H. Greenaway, and D. P. Towers. 2006. Wavefront sensing for single view three-component three-dimensional flow velocimetry. *Experiments in Fluids* 41 (6):881-891.

Bown, M. R., J. M. MacInnes, R. W. K. Allen, and W. B. J. Zimmerman. 2006. Three-dimensional, three-component velocity measurements using stereoscopic micro-PIV and PTV. *Measurement Science & Technology* 17 (8):2175-2185.

Chen, S., N. Angarita-Jaimes, D. Angarita-Jaimes, B. Pelc, A. H. Greenaway, C. E. Towers, D. Lin, and D. P. Towers. 2009. Wavefront sensing for three-component three-dimensional flow velocimetry in microfluidics. *Experiments in Fluids* 47 (4-5):849-863.

Cierpka, C., R. Segura, R. Hain, and C. J. Kähler. 2010. A simple single camera 3C3D velocity measurement technique without errors due to depth of correlation and spatial averaging for microfluidics. *Measurement Science & Technology* 21 (4):045401.

Cierpka, C., R. Segura, M. Rossi, and C. J. Kähler. under review. Theoretical and experimental investigation of astigmatism μ–PTV. *Exp. Fluids*.

Cierpka, C., T. Weier, and G. Gerbeth. 2008. Evolution of vortex structures in an electromagnetically excited separated flow. *Experiments in Fluids* 45 (5):943-953.

Duncan, J., and et al. 2010. Universal outlier detection for particle image velocimetry (PIV) and particle tracking velocimetry (PTV) data. *Measurement Science and Technology* 21 (5):057002.

Hain, R., C. J. Kähler, and R. Radespiel. 2009. Principles of a volumetric velocity measurement technique based on optical abberations. *Notes on Numerical Fluid Mechanics and Multidisciplinary Design* 106:1-10.

Kähler, C. J. 2004. The significance of coherent flow structures for the turbulent mixing in wall-bounded flows, DLR Research report, FB 2004-24, ISSN 1434-8454, 2004: DLR, http://webdoc.sub.gwdg.de/diss/2004/kaehler/kaehler.pdf.

Kähler, C. J., R. J. Adrian, and C. Willert. 1998. Turbulent boundary layer investigations with conventional and stereoscopic particle image velocimetry. Paper read at 9th International Symposium on Applications of Laser Techniques to Fluid Mechanics, June 13-16, at Lisbon, Portugal.

Kim, S., and S. J. Lee. 2009. Measurement of Dean flow in a curved micro-tube using micro digital holographic particle tracking velocimetry. *Experiments in Fluids* 46 (2):255-264.

Lee, S. J., and S. Kim. 2009. Advanced particle-based velocimetry techniques for microscale flows. *Microfluidics and Nanofluidics* 6 (5):577-588.

Lindken, R., M. Rossi, S. Grosse, and J. Westerweel. 2009. Micro-Particle Image Velocimetry (mu PIV): Recent developments, applications, and guidelines. *Lab on a Chip* 9 (17):2551-2567.

Lindken, R., J. Westerweel, and B. Wieneke. 2006. 3D microscale velocimetry methods: A comparison between 3D-μPTV, stereoscopic μPIV and tomographic μPIV. Paper read at

13th Int. Symp. on Applications of Laser Techniques to Fluid Mechanics, June 26-29, at Lisbon, Portugal.

Maas, H. G., A. Gruen, and D. Papantoniou. 1993. Particle Tracking Velocimetry in 3-Dimensional Flows .1. Photogrammetric Determination of Particle Coordinates. *Experiments in Fluids* 15 (2):133-146.

Olsen, M. G., and R. J. Adrian. 2000. Out-of-focus effects on particle image visibility and correlation in microscopic particle image velocimetry. *Experiments in Fluids* 29:S166-S174.

Ooms, T. A., R. Lindken, and J. Westerweel. 2009. Digital holographic microscopy applied to measurement of a flow in a T-shaped micromixer. *Experiments in Fluids* 47 (6):941-955.

Pereira, F., M. Gharib, D. Dabiri, and D. Modarress. 2000. Defocusing digital particle image velocimetry: a 3-component 3-dimensional DPIV measurement technique. Application to bubbly flows. *Experiments in Fluids* 29:S78-S84.

Ragan, T., H. D. Huang, P. So, and E. Gratton. 2006. 3D particle tracking on a two-photon microscope. *Journal of Fluorescence* 16 (3):325-336.

Rossi, M., C. Cierpka, R. Segura, and C. J. Kähler. 2010. On the effect of particle image intensity and image preprocessing on depth of correlation in micro-PIV measurements. Paper read at International Symposium on Applications of Laser Techniques to Fluid Mechanics, 5-8. July, at Lisbon, Portugal.

Santiago, J. G., S. T. Wereley, C. D. Meinhart, D. J. Beebe, and R. J. Adrian. 1998. A particle image velocimetry system for microfluidics. *Experiments in Fluids* 25 (4):316-319.

Sun, Y., S. Duthaler, and B. J. Nelson. 2004. Autofocusing in computer microscopy: Selecting the optimal focus algorithm. *Microscopy Research and Technique* 65 (3):139-149.

van Hinsberg, N. P., I. P. Roisman, and C. Tropea. 2008. Three-dimensional, three-component particle imageing using two optical aberrations and a single camera. Paper read at 14th International Symposium on Applications of Laser Techniques to Fluid Mechanics, July 7-10, at Lisbon, Portugal.

Westerweel, J., and F. Scarano. 2005. Universal outlier detection for PIV data. *Experiments in Fluids* 39 (6):1096-1100.

Willert, C. E., and M. Gharib. 1992. 3-Dimensional Particle Imaging with a Single Camera. *Experiments in Fluids* 12 (6):353-358.

Yoon, S. Y., and K. C. Kim. 2006. 3D particle position and 3D velocity field measurement in a microvolume via the defocusing concept. *Measurement Science & Technology* 17 (11):2897-2905.